



The 1895 Ljubljana earthquake: source parameters from inversion of macroseismic data

Franco Pettenati · Ivana Jukić · Livio Sirovich · Ina Cecić · Giovanni Costa · Peter Suhadolc

Received: 6 April 2023 / Accepted: 15 November 2023
© The Author(s) 2024

Abstract The 14 April 1895 (Mw 6.1, in the area of Ljubljana, Slovenia) earthquake is still not fully understood. The aim of this work is to derive information about its source from the inversion of an updated dataset of intensities (evaluated with EMS-98). This was done via automatic non-linear geophysical inversion *KF-NGA*, which was performed using a Niching Genetic Algorithm and has been presented in other articles. The distribution of damage caused by this earthquake is not homogeneous and often shows significant intensity differences between neighbouring sites. Statistical analysis of the intensities, epicentral distances and geologic nature of the sites suggests some site effects. Nevertheless, the resulting solution is consistent with regional seismotectonics, i.e. an almost pure dip-slip mechanism: strike $282^\circ \pm 5^\circ$, dip

$38^\circ \pm 7^\circ$, rake $86^\circ \pm 9^\circ$ ($\pm 180^\circ$ because of the intrinsic ambiguity of the *KF-NGA*-inversion). Since the rake angle is close to 90° , there is an almost perfect ambiguity between the two planes of the focal mechanism. Therefore, our solution has a Dinaric direction and could be associated either with a fault plane that dips NE or with one that dips SW.

Keywords Ljubljana earthquake of 1895 · Kinematic function · Source inversion · Macroseismic intensity · Site effects

1 Introduction

The area of Ljubljana (Fig. 1), Slovenia, is affected by moderate (Bavec et al. 2012; Šket-Motnikar et al. 2022) seismicity that has resulted in historic earthquakes such as the Ljubljana Earthquake (Mw 6.1)

Supplementary Information The online version contains supplementary material available at <https://doi.org/10.1007/s10950-023-10178-0>.

F. Pettenati (✉)
Istituto Nazionale Di Oceanografia E Di Geofisica
Sperimentale, OGS, Borgo Grotta Gigante, 42/C Sgonico,
34010 Trieste, Italy
e-mail: fpettenati@ogs.it

I. Jukić
International Data Centre, Comprehensive Nuclear-Test-Ban Treaty Organization (CTBTO), Vienna International Centre, P.O Box 1200, 1400 Vienna, Austria

L. Sirovich · P. Suhadolc
34100 Trieste, Italy

I. Cecić
Ministrstvo Za Okolje, Prostor in Energijo, Agencija
Republike Slovenije Za Okolje, ARSO, Vojkova 1B,
1000 Ljubljana, Slovenia

G. Costa
Dipartimento Di Matematica E Geoscienze, University
of Trieste, SeisRaM Group, Via Weiss 2, 34100 Trieste,
Italy

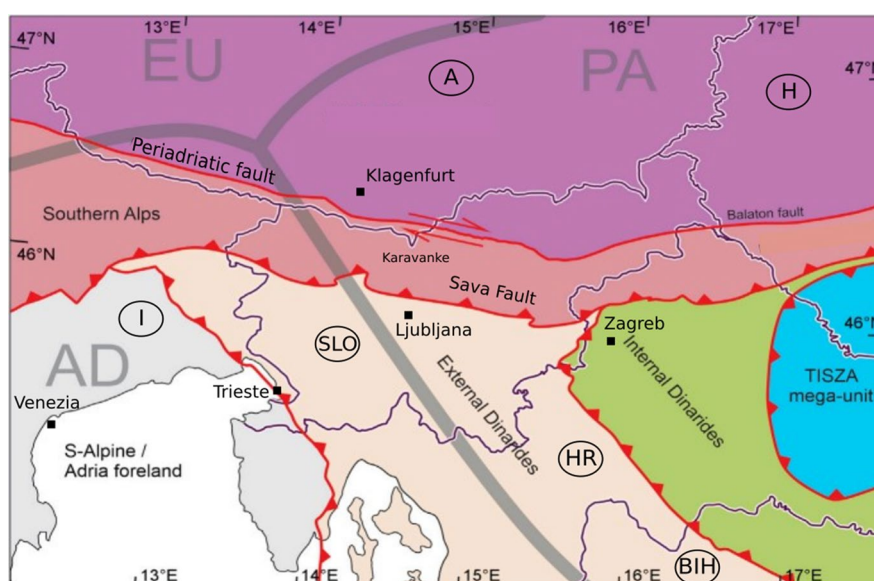
on 14 April 1895. This earthquake significantly damaged the city (Imax VIII-IX EMS-98, Cčić, 1998a) and was followed by a long series of aftershocks, the strongest of which was the one on 15 July 1897 (Mw 5.0, Imax VII EMS-98, Cčić, 1998b). The epicentral area is the most densely populated area in Slovenia (with currently more than 300,000 inhabitants). The quake was also felt in neighbouring countries: in northern and central parts of Italy, as far as Umbria and Tuscany, in Austria including Vienna, in western Hungary, in almost all of Croatia and in Bosnia and Herzegovina.

First Ribarič (1982) and then Rovida et al. (2020, i.e. the CPTI15 catalogue) proposed the epicentral coordinates of the earthquake under study (Fig. 2), using the intensity (I hereafter) databases available to them at the time. Ribarič's (1982) estimates are $M_m=5.8$ or $M_w=6.1$; epicentre coordinates 14.50E and 46.10N; depth 16 km and an observed maximum intensity I_0 VIII-IX. Rovida et al. (2020) suggested $M_w=6.0$; 14.514E, 46.125N for epicentre and I_0 VIII. The two assessments are comparable, only the magnitude and I_0 of Rovida et al. (2020) are slightly underestimated, but these authors distinguish three aftershocks that occurred within an hour and M_w around 4.2–5.0. To calculate the magnitude and epicentre, the former author adopted the consolidated method using isoseismals (epicentral intensity I_0 , rays and depth), while the latter authors used the Boxer method (Gasperini et al. 2010).

The knowledge of the 1895 earthquake and its source can influence the modern calculation of hazard also for the large urban area of Ljubljana. The first twenty-first century, seismic hazard map of Slovenia (Lapajne et al. 2003) was prepared using the “Smoothed Seismicity” method (Frankel 1995), which avoids the delineation of any seismic sources, because the maps are based only on historical seismicity. The authors of this map did not even take the characteristic earthquake into account, since there was no clear evidence of characteristic earthquakes in Slovenia at that time. In particular, when looking at the western side of the hazard map for Slovenia, the problem of the epicentre of the 26 March 1511 earthquake arises, the location of which is still debated (e.g. Fitzko et al. 2005, M 6.9; Camassi et al. 2011; Rovida et al. 2020 CPTI15, Mw 6.3). This is the strongest historical earthquake in the border area with Italy and affects the hazard estimates for both regions. See Section 1.1 for the details. To the E, on the other hand, two historical earthquakes play an important role in the hazard calculation of the Krško NPP: 1880 (M 6.3, Herak et al. 2009) and 1917 (M 5.7, Ribarič 1982, who used eight stations; M 6.2, Grünthal and Wahlström 2012, Atanackov et al. 2021). Recently, Šket-Motnikar et al. (2022) presented a new probabilistic seismic hazard (PHSA) map in the context of Cornell (1968).

The objective of this paper is to search for the fault source of the 1895 Ljubljana earthquake. Therefore, we present below the seismotectonics of the target

Fig. 1 Map of the general structure and regional tectonic subdivision of Slovenia and its surroundings. Modified map from Atanackov et al. (2021), with suggestions from Žibret and Vrabec (2016). The thick gray lines represent the boundary between the European plate (EU), the Adria microplate (AD) and the Pannonian Domain (PA)



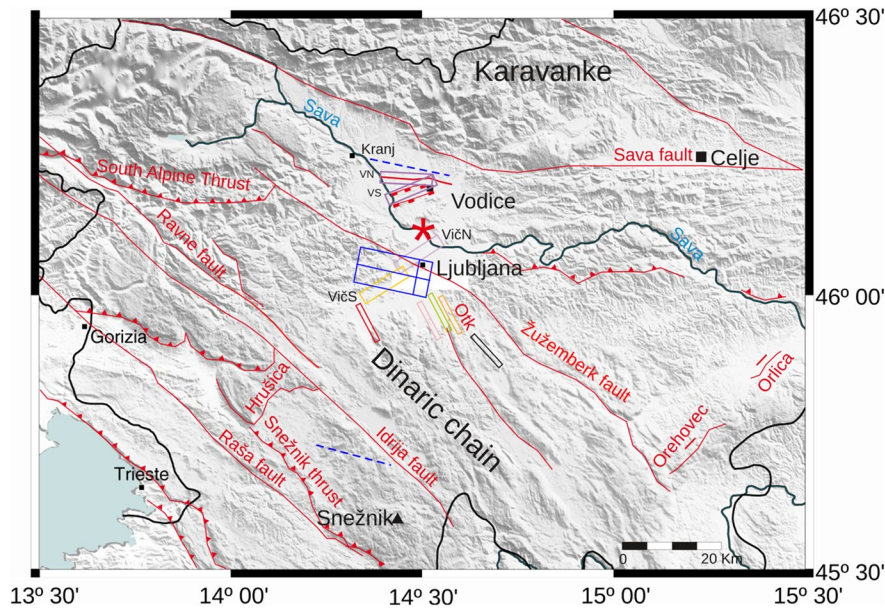


Fig. 2 Tectonic map of the study area (from Žibret and Vrabec 2016). Vodice faults are taken from Vrabec (2001). The red star is the Ribarič's (1982) macroseismic epicentre. The epicentre of the CPTI15 catalogue is located near the red star, slightly to the northeast. The blue box is the fault proposed in this study (Table 3 — deme 2), while the other boxes are the faults considered in Tiberi et al. (2018): dark purple Vodice S (VS) and Vodice N (VN); light purple Vič N; yellow Vič S; red

Borovnica; pink Mišjedolski; light green Želimlje; orange Ortnik (Otk); black Dobrepolje. The blue dashed line in the south of the box of deme 2, is the intersection between the upward virtual continuation of deme 2 plane, dipping 38° to NNE and the topographical surface. Similarly, the blue dashed line in the north is the intersection with the topographic surface of the plane prosecution of the conjugate plane of deme 1 dipping 52° to SSW

region (Section 1.1) to check the compatibility with the solution. The study applies the *KF-NGA* inversion procedure, which uses macroseismic intensity “points”, as data, commonly referred to as *MDPs* (i.e. related to an inhabited location), described in Section 2. This procedure is based on the kinematic function (*KF*) approach (Sirovich 1996; Sirovich and Pettenati 2004; Pettenati and Sirovich 2007) and is described in Section 3. The *I* used here (evaluated with EMS-98 European Macroseismic Scale, Grünthal 1998) were analysed and reviewed by I. Cecić of the Slovenian Environmental Agency (ARSO), using the funds in the ARSO Macroseismic Archive; hereafter: ARSO (2012).

Before performing the inversions, we analysed the intensities *I* as a function of the epicentral distance *d* and the soil properties from different site catalogues in Section 2.3 (Pettenati et al. 2012). Despite the availability of a large amount of data on soils, this analysis was hampered by poorly organised and chaotic distribution of *I* data. After analysing

and processing the data and eliminating outliers, we inverted the dataset with the *KF-NGA* method.

1.1 Tectonics of the Ljubljana area

The interpretation of the seismotectonics of Slovenia, northern Croatia and adjacent areas is in rapid evolution. The literature is not unanimous, either in the choice of the names of microplates, crustal blocks and units or in the geodynamic and palinspastic reconstructions (sensu Kay 1937). The area lies at the end of the Dinaric chain (Figs. 1 and 2) and includes the easternmost part of the Southern Alps, bordering the Pannonian Basin to the E. This area of the Southern Alps is called Karavanke and borders the plain (Fig. 2), which is crossed by the Sava River in the south. The river flows parallel to the Periadriatic Suture, along a tectonic line called the Sava Fault. This line defines the northern Ljubljana Basin, which forms the boundary between the Southern Alps and the Dinarides (Placer 2008) (Fig. 2). In the Ljubljana

Basin, two distinct areas meet in the Sava Plain: to the N is an area with a series of Dinaric structures, mainly thrusts with the direction WNW-ESE (Placer et al. 2010); further SE, there is the area of the Sava Folds, affected by WSW-ENE-oriented structures, mainly folds but also with some important transcurrent faults, usually sinistral, such as the Orehovec and Orlica faults (Atanackov et al. 2021). This is a transition zone between (clockwise description – Fig. 2): (1) the eastern foothills of the Southern Alps, in contact with the Pannonian Basin; (2) the eastern Sava Graben area — often referred to as the Balaton Zone or the Tisza microplate — with moderate present-day seismic activity and (3) the Dinarides, extending from E to W: (3i) the inner Dinaric thrusts, (3ii) the external Dinaric thrusts and (3iii) the chain of the external thrusts with an imbricated structure (Dalmatian coast and islands) (see Placer et al. 2010).

In western Slovenia, the Dinaric Fault system consists of a NW–SE trend of active right-lateral strike slip faulting (Žibret and Vrabc 2016; Atanackov et al. 2021; Grützner et al. 2021). Formed during the Cenozoic, this system is the junction of the Dinaric chain with the Alps and accommodates the northward movement of the Adria plate with respect to Eurasia. Although the system produces moderate earthquakes, it is largely unknown whether Late Quaternary faulting also produces strong earthquakes. Grützner et al. (2021) point out a difficulty in understanding the regional tectonics and the seismic hazard of the area. Indeed, Žibret and Vrabc (2016) report two main thrust characteristic of this area and at least four post-Paleocene stress tensor groups. This area, with a system of active faults, represents one of the main sources of seismic hazard in Slovenia (Vičič et al. 2019). Eastern Slovenia is also influenced in the south by the External Dinarides (Poljak et al. 2000), while the north eastern part lies within the Pannonian Basin, with a system of left-lateral strike-slip faults trending toward ENE-WSW and intersecting the Dinaric lineaments in the southern part (NW–SE).

In the middle, the Ljubljana Basin is bounded on the N by the east–west striking dextral fault, the Sava Fault (Fig. 2) and crossed by the Žužemberk Fault (Vrabc and Fodor 2006). GPS measurements suggest that the Sava Fault is currently active at a slip rate of $\sim 1 \text{ mm a}^{-1}$ (Vrabc and Fodor 2006). Smaller \sim E-W-oriented reverse faults displacing Quaternary sediments in the

basin (Verbič 2006) may indicate a recent change in deformation regime from transtensional subsidence to transpression (Jamšek Rupnik et al. 2013). There are opposing interpretations related to the Ljubljana Basin (Jamšek Rupnik et al. 2013) and the Sava folds area (Vrabc and Fodor 2006). The Ljubljana Basin is interpreted as a transpressional zone, with dextral strike-slip movement along NE-SW faults and overthrust along minor structures EW. The Sava Fold is considered to be an area dominated by E-W to ENE-WSW trending synclines of Neogene strata. The synclines formed between uplifts of the pre-Tertiary basement, which were uplifted along moderately dipping reverse faults.

In the inner and external Dinarides, the presence of strike-slip or transpressive dextral large faults is significant, some of which exhibit seismic activity today. In particular, one of these faults, although not the largest, the Ravne fault, was responsible for the two Bovec earthquakes of 1998 (M_s 5.7) and 2004 (M_s 5.1) (Bajc et al. 2001; Vičič et al. 2019). The 26 March 1511 earthquake with a magnitude of $M=6.9$ was attributed to the Idrija fault (Fitzko et al. 2005) but was recently located westward in the Friuli-Venezia Giulia region (Italy) on a Dinaric lineament, as a continuation of the Idrija fault (Camassi et al. 2011; Rovida et al. 2020 CPT15). Another fault with a maximum magnitude of 7 is attributed to the Orlica fault (Sirovich et al. 2012). Such structures may represent a high seismic potential.

As for the Southern Alps, their eastern boundary is disputed, but at present, they seem to meet the Dinarides (although the contact between the Alps and the Dinarides cannot always be established with certainty). It should be noted that the Balaton zone mentioned above does not coincide exactly with the “Pannonian suture” (after Poljak et al. 2000). Unfortunately, GPS measurements are still scarce in the region. From the GPS-derived motions of Weber et al. (2010), we know that the Adriatic microplate is moving northward, but we cannot distinguish what is going on in the transition region under study.

The epicentral area of the 1895 earthquake is in the Ljubljana Basin (Fig. 1), for which there is extensive knowledge and discussion regarding the active faults. The tectonic context is of active deformation in a releasing overstep between NW–SE-striking dextral strike-slip faults that generated and bounded the pull-apart basin, with blocks dipping along normal

faults (Vrabec 2001; Vrabec and Fodor 2006). The Ljubljana Basin is filled with Quaternary sediments reaching a thickness of up to 280 m in some parts. However, in this context, Jamšek Rupnik (2013) and Jamšek Rupnik et al. (2015) interpret the two small WSW-ENE-striking faults of Vodice S, which are 11 km long and located 15 km N of the Slovenian capital (see their location in Fig. 2), as reverse dipping NNW. These authors base their interpretation on the topographic profiles of the Vodice fault scarps (Fig. 6.2 Profile N.3, in Jamšek Rupnik 2013 not shown here) and on a paleoseismological trench with ^{14}C and optical stimulation luminescence OSL datings.

Jamšek Rupnik et al. (2013) also evaluated movements along the scarp in question, which offsets Quaternary sediments, ranging from 5 to 25 m in height over a length of 10 km. Their interpretation of the deformations is also based on geomorphological evidence of the evident folds in the Quaternary sediments, in a clay pit at the eastern end of the escarpment and in the conglomerates of the Sava bank in the western part of it, where the fault intersects the river. In this way, they calculated a sliding velocity of 0.2–0.4 mm/year, expecting an earthquake of magnitude 6.2–6.3. In our opinion, however, the interpretation of the two aforementioned scarps as normal, dipping SSE, is still not precluded.

2 Data analysis

2.1 Macroseismic data of 14 April 1895

In order to obtain a good dataset, we solved numerous problems related to place toponymy in the macroseismic data points file (Cecić, 1998a), since many towns or villages had other official names almost 130 years ago, either in German or Italian language.

The macroseismic information was taken from these historical databases:

- Slovenian catalogue, for the 1895 event, ARSO (2012; data set for this earthquake published in Cecić, 1998a). Intensities I are evaluated using the EMS-98, with some data points converted to MSK scale from a previous database, and also integrated with new data.
- The Italian parametric catalogue CPTI11 (then) CPTI15 (Rovida et al. 2020) of INGV (National Institute of Geophysics and Vulcanology, Rome). This catalogue uses the Mercalli Cancani Sieberg scale (MCS).

For the 1895 event, we used the ARSO (2012) catalogue for data from Slovenia, Italy, Austria, Hungary, Croatia and Bosnia-Herzegovina, while we used the Italian CPTI15 catalogue for sites in Italy and other countries not included in the ARSO (2012). Before merging the data into the dataset used for the 1895 inversion, we compared 25 intensities of the Italian territory, included in both catalogues but in two different scales, using the scatter plot in Fig. 3a. The Italian catalogue (on y-axis) slightly overestimates the low degrees. Regarding the uncertainties arising from the use of the two different scales, we are satisfied — as a first approximation — with the authoritative opinion of three renowned experts (Musson et al. 2010): “Ideally, direct conversion between intensity scales should never be made” but, “these values are likely to vary more between two seismologists using the same scale than between two scales used by the same seismologist”. A more recent study (Vannucci et al. 2021), for the Italian catalogue, shows a difference of half a degree on average between EMS and MSC scales. What is shown in Fig. 3a is consistent with these last authors. Since the current work deals with an 1895 earthquake, the vulnerability of buildings is only class A (most) and B (few), so MCS and EMS should give very similar values for the intensities (see Fig. 2 in Del Mese et al. 2023).

2.2 Merged dataset

As a result, we used a dataset of 1004 MDPs with intensities from VIII–IX to II–III (see Supporting Information (Fig. S1)- the data in the Spreadsheet1). In the ARSO (2012) catalogue, there are 15 localities with uncertain estimates, between V and VI degrees, not evaluated V–VI but with the real number “5.6”. We rounded them to VI for three reasons: (i) the general code is “damage”; (ii) to be conservative in accounting for uncertainty; (iii) some of the sites with these uncertainties are located in the epicentral area (see Section 2.4). Since most of the data are in the EMS-98 scale, we chose to use “intermediate degrees” (i.e. for VI–VII we use 6.5). The reason for this is that there

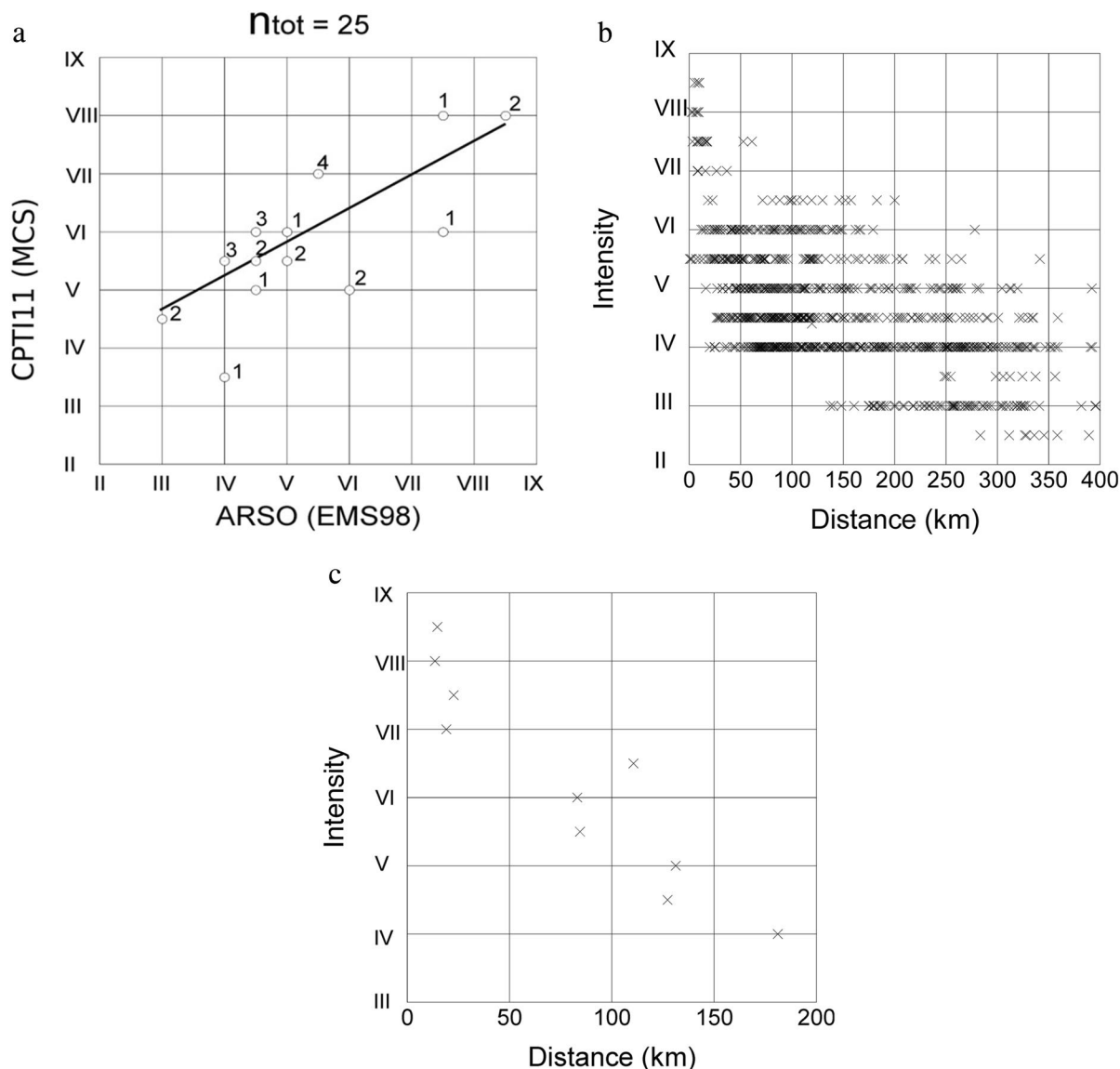


Fig. 3 **a** Scattergram of correlation of 25 sites (n_{tot}) in scale EMS-98 and MCS. The numbers indicate how many intensities are represented by each point. **b** Plot of intensity decay with distance d for GMPE representation. All data (1004 MDPs) from both ARSO (2012, in the EMS-98 scale) and CPTI15

(Rovida et al. 2020 MCS scale) datasets. **c** Intensity decay for average distance d for Slovenian and Croatian data within 200 km. There is an anomalous trend in the range IV–V to VI–VII. This may be due to the presence of many Croatian data at d s greater than 60 km (state boundary)

may be equiprobability between the two degrees in question if the diagnosis is unclear. The EMS-98 scale is designed to better account for building typology, and there may be uncertainty in the range of values if the two degrees in question correspond to two different typologies (Tertulliani, 2021, private communication). In the case of the used dataset of 1004 MDPs, there is a significant uncertainty due to local effects.

2.3 Statistics of the dataset

Figure 3 b shows the decay of I with epicentral distance d for 1004 MDPs. The scatter of the data is typical for this kind of graphical representation, especially for data $I < VII$. In particular, there is a noticeable concentration of sites with degree V–VI, very close to the epicentre, likely also because of the 15 ARSO (2012) localities

with uncertain estimates mentioned in Section 2.1. In Fig. 3c, we have tried to better show the decay of I with respect to the average d for all intensity classes. It is confirmed that in this case, the I does not decrease regularly with the increase of d . The average d of the VIII degree is slightly lower than that of VII, VII–VIII and VIII–IX, but the anomaly is most evident in the range IV–V to VI–VII. Much of the data from VI and VI–VII are from the Croatian territory, at d greater than 60 km (state border); however, similar intensities I are also found in Slovenia, so a systematic bias due to different survey practices is excluded. The large average d value

of VI–VII is limited by a small number of data (Fig. 3b) compared to the large dataset of III to VI.

To check for the presence of outliers in the dataset, we applied the classic Chauvenet method (Barnett and Lewis 1978), which has been used in previous articles (Sirovich and Pettenati 2004; Pettenati and Sirovich 2007). For this dataset, six outliers were found and removed from the inversion (see in Table 1). With the exception of the Oradea site ($I=III$), all outliers are at the shortest d of their classes. Instead, Oradea is on the largest d of its class (> 500 km). Figures 4a and b show the number of sites by d and by I : V in Fig. 4a, VI in Fig. 4b.

Table 1 The identified outliers $ds=log(d)$, and related I , in the 1895 dataset

Intensity	Outlier d (km)	Coordinates	Locality
VI-VII	22.77	45.813 N–14.380 E	Begunje (SLO)
VI-VII	18.26	45.837 N–14.470 E	Pirmane (SLO)
V-VI	0.66	45.998 N–14.508 E	Brest (SLO)
V	16.22	45. 878 N–14.615 E	Turjak (SLO)
IV	19.91	45.892 N–14.705 E	Čušperk (SLO)
III	582.50	47.060 N – 21.932 E	Oradea (ROM)

2.4 Site effects

In general, clustered site effects would affect the inversion; instead, isolated and sparse site effects increase the noise but should not significantly affect the results. However, if the intent is to correct I for local effects, then a valid criterion is needed for all sites. Otherwise, if only specific site values are corrected, there is a risk of criticism of checking only selected data or modifying these data to steer the

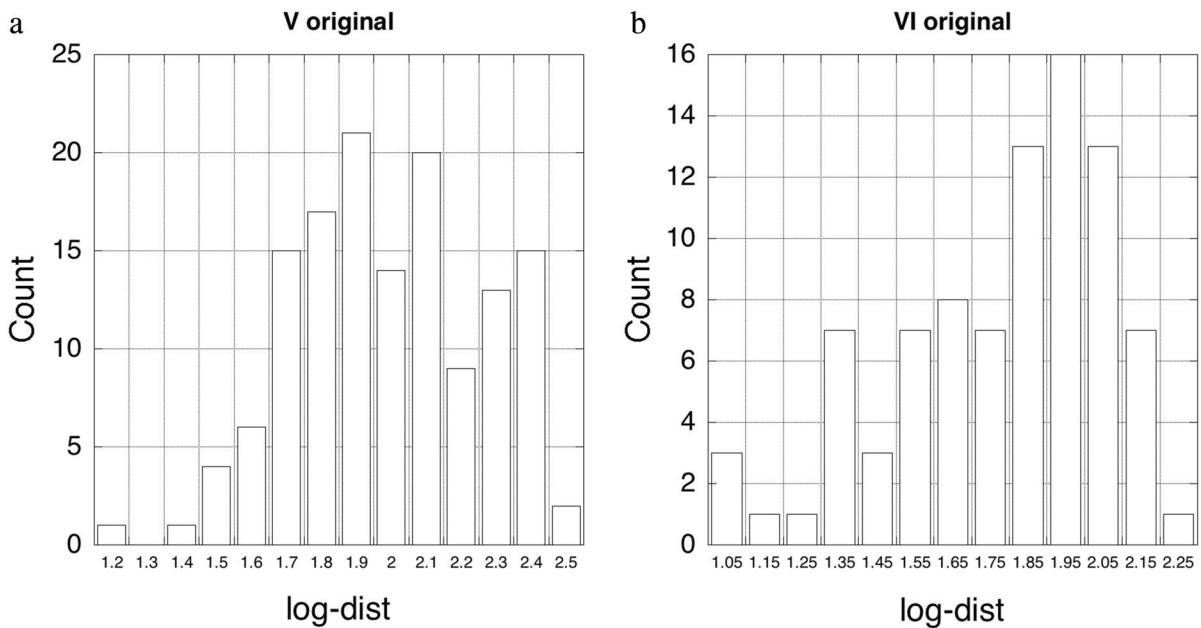


Fig. 4 **A** Distribution of data points with intensity V with an outlier at the shortest d . **b** Distribution of data points with intensity VI with an outlier at the shortest d . One of the three data in the first bin

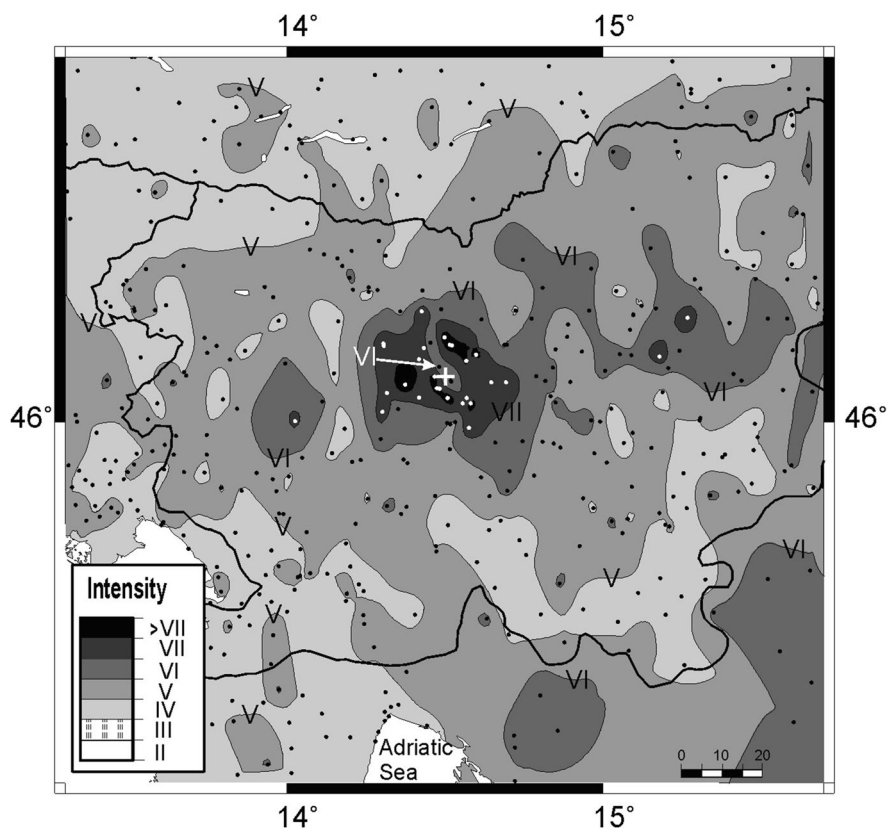
inversions to the desired results. Stating that these corrections were made to site-specific studies by other authors would not be sufficient. No specific site effects studies are available for the 1895 event.

To reinforce the decision not to use user-defined corrections, it is worth noting here that in inversion procedures, de-amplifications generally have the same importance as amplifications. In the meizoseismic area of Fig. 5, the VI isoseismal splits the areas of highest degrees, with three intensity VI sites aligned from N to S (see the white arrow in the figure). Here, however, all sites from V–VI to VIII fall into the soft soils categories. Therefore, it is difficult to argue that the aforementioned three VI sites have de-amplification due to their soil properties. Rather, this minimum I may be a source effect, as we have demonstrated for the 2009 Chino Hills earthquake (Sirovich et al. 2009). Further comments on this argument are reported in Section 5. Unfortunately, we cannot make a more rigorous hypothesis in the present case because of the too small distance d from the source for our model.

To analyse the presence of local effects, we used the pattern followed in other works. We performed $d(I)$ regressions as in Pettenati and Sirovich (2003, see p. 50 and Fig. 3) and in Pettenati and Sirovich (2007 see p. 1592, Fig. 3). Thus, the distances of the sites were subdivided according to the geology of the sites (Jamšek Rupnik, 2012, written communication — Pettenati et al. 2012). For this purpose, a simple classification was used: rock; stiff soil; soft deep soil; soft shallow soil, as in Pettenati et al. (2018, see Fig. 6, page 454). 95% confidence bands of $(d(I); I)$ regression lines were used as a statistical criterion to distinguish MDP populations with different soils. In this way, 310 sites of the whole dataset, entirely derived from Slovenian and Croatian data, were classified in the following categories, as in Pettenati et al. (2012):

- A sound rock, Carboniferous, Permian and Mesozoic carbonate and clastic rocks, schists and phyllites included shear-wave velocity $V_S > 1500$ m/s

Fig. 5 The 431 MDP values from the two datasets ARSO (2012, in scale EMS-98) and CPTI15 (Rovida et al. 2020, MCS scale for Italian data), interpolated by the N–N method and contoured. The epicentre from Ribarič (1982) is marked with a white cross. The white arrow indicates the anomaly of the three VI degree sites



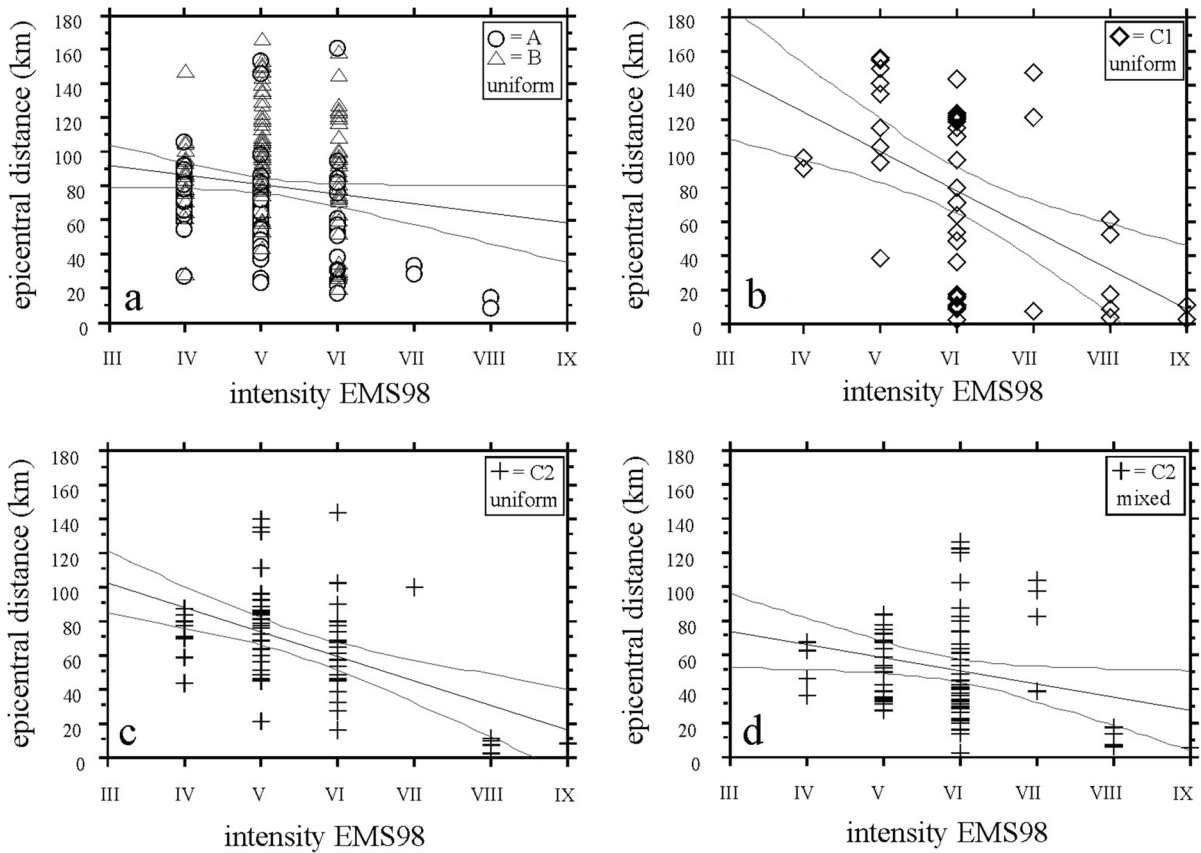


Fig. 6 Site effects study on 310 sites of the entire dataset, derived from Slovenian and Croatian data (Pettenati et al. 2012), and classified according to the following categories (Jamšek, 2012, written communication): (A) sound rock, Carboniferous, Permian and Mesozoic carbonate and clastic rocks, schists and phyllites included shear-wave velocity $VS > 1500$ m/s; (B) stiff, $400 < VS \leq 1500$ m/s, soft rocks, very dense soils, Flysch, Miocene organic limestone (“*Litotamnijski apnenec*”), clastic rocks

- B stiff, $400 < VS \leq 1500$ m/s, soft rocks, very dense soils, Flysch, Miocene organic limestone (“*Litotamnijski apnenec*”), clastic rocks and very consolidated sediments of Oligocene-Pleistocene conglomerate, tuffs and tuffites
- C1 soft, mostly alluvium (gravelly, sandy, silty, clayey) $VS \leq 400$ m/s, thickness $t > 30$ m
- C2 like C1 but $t \leq 30$ m. Highly heterogeneous and/or uncertain sites were omitted, but C2 also contained loess, colluvium, muds, diluvium and moraines

Classes A and B were grouped together for statistical reasons. This appears to be a common case, as

and very consolidated sediments of Oligocene-Pleistocene conglomerate, tuffs and tuffites; (C1) soft, mostly alluvium (gravelly, sandy, silty, clayey) $VS \leq 400$ m/s, thickness $t > 30$ m; (C2) like C1 but $t \leq 30$ m. (or uncertain sites were omitted) (it emerged that C2 also contained loess, colluvium, muds, diluvium, and moraines). Note the lower attenuation of C1 sediments, with respect to the other categories

the same grouping was required for the California dataset mentioned above.

We analysed the three groups of sites with uniform geology (i.e., homogeneous of outcrop) separately; in the fourth group, we retained the mixed sites with a predominant outcrop; it appeared that the only mixed group with sufficient data was the one with dominant C2 (soft, $t \leq 30$ m). Therefore, the highly heterogeneous and/or uncertain sites were omitted from the analyses. (Fig. 3 of Tiberi et al. (2018) shows the geographic distribution of these data.

Despite this dispersion, I decreases with d faster in rocky and stiff sites (Fig. 6a) than at sites with deep soft sediments (Fig. 6b), with shallow soft sediments

showing intermediate behaviour (Fig. 6c), but closer to categories A+B than to C1. This could suggest that local soft sedimentary cover may have a minor influence (although this is not consistent with other observations elsewhere that emphasised the amplification capacity of 15–30-m-thick soft sedimentary covers: Pettenati and Sirovich 2007; Pettenati et al. 2018). The problem of class C2 for thickness ≤ 30 m is highlighted in Paolucci et al. 2021, who attest: “The most relevant discrepancies occur for the shallow soft soil conditions (soil category E)”. Finally, the mixed sites (sites with predominant C2; see Fig. 6d) show a similar gradient as in Fig. 6a, but with lower ordinates than in Fig. 6a given the structure of the regressions in Figs. 6; this implies somewhat lower intensities compared to rocky and stiff sites for all d ranges. Further comments on this can be found in Section 5.

3 KF inversion method

3.1 KF model

For the radiation model in this work, we use the KF formula (Sirovich 1996, 1997; Sirovich and Pettenati 2004; Pettenati and Sirovich 2007):

$$KF(P, l) = \frac{R(P, l)}{D(P, l) \left[1 - \left(\frac{V_s}{V_p} \right) \cos \theta(P, l) \right]} \quad (1)$$

KF considers body-wave radiation of a source point of dislocation, propagating horizontally along a linear fault on a rupture plane of unit width at depth H and distance l from the nucleation point, to the displacement-related ground motion at the receiver point P on the surface at distance $D(P, l)$ and angle $\theta(P, l)$ between rupture direction and ray to P . $R(P, l)$ is the radiation pattern of S-waves. KF uses an elastic half-space in the distance range of about 5 to 100 km from the source, and wavelengths shorter than the shortest distance between the observer and the source. KF agrees with the asymptotic approximation (Madariaga and Bernard 1985).

The KF model uses 11 source parameters adopting the convention of the positive direction of the strike ranging from 0° to 360° , with the fault plane dipping to the right. According to this, rake angles ranging between 1° and 179° indicate faults with reverse

(compressive) components. In our convention, the total length of the rupture is the sum of the absolute values of the parts along-strike (considered positive $L+$) and antistrike (negative $L-$). The same goes for the Mach number (Mach+, and Mach-). L is derived from M_0 , by the empirical relationship M versus RLD (Wells and Coppersmith 1994) for all types of faults

$$\log(\text{RLD}) = 0.59M - 2.44 \quad (2)$$

We do not describe again the whole procedure, but only point out that the results are nondimensional values of $KF(x, y)$ at locations x, y (referred to a Cartesian plane). The $KF(x, y)$ data are then converted to *pseudo-intensities* by the semi-empirical data-fitting function in (2) (Sirovich et al. 2001; Pettenati and Sirovich 2003).

It should also be kept in mind that our KF method is unable to distinguish between the results of mechanisms that differ in the rake angle by 180° , since it produces the same radiation but with reversed polarities in both cases. This ambiguity can only be resolved by instrumental records or additional tectonic/geodynamic information. Secondly, our KF inversion problem is close to bimodality in the case of almost pure dip-slip mechanisms (Gentile et al. 2004).

3.2 Genetic algorithm

The search for the absolute minimum variance model of source parameters model space was performed with a sharing Niching genetic algorithm (NGA) (Martin et al. 1992), using the parallel genetic algorithm library routines by Levine (1996) and four separate subpopulations (Deme). Each deme has 1000 sources and evolves independently from the others, because in this step, the normalised distance “ D ” (see Gentile et al. 2004, page 1741), between each source of a deme and each source of all the other sub-populations, obeys a certain condition (Eq. 1 of Koper et al. 1999). Since our NGA inversion technique has already been presented (Gentile et al. 2004; Sirovich and Pettenati 2004; Pettenati and Sirovich 2007), we refer the reader to these publications for details. To follow the asymptotic approximation, all sites closer than 5 km to the epicentre were assigned the maximum *pseudo-intensity* value of the site closest to the source, but outside the 5-km range, or less than an intensity limit assigned as input parameter. Finally, the selected objective

function during the inversion was $\sum r_s^2$, where r_s is the observed $I (I_{\text{obs}})$ minus the *pseudo-intensity* calculated at a site (the suffix denotes the sites). The uncertainties of our inversion results correspond to the incremental variation steps shown in Table 2. The table also shows the ranges examined. As can be seen here, no constraints were assumed for the fault-plane solutions and for the nucleation location (in the latter case some limits are obvious), and large ranges have been chosen for the other parameters.

3.3 Inversion errors

The *KF* inversion is a typical example where the calculation of the inversion error is mathematically difficult because different sets of I_{obs} values are not available. Therefore, the inversion errors were calculated using a randomization by the Monte Carlo technique as performed for three earthquakes in California (Pettenati and Sirovich 2007) and two in Italy (Sirovich et al. 2013). For each source parameter, a random number N ($50 < N < 250$) of artificial intensity datasets were created. All sites were then assigned new I , and each artificial set was assembled under the following conditions.

The artificial values must lie within the I–XI limits. Assuming a normal distribution centred on the observed I_{obs} value with a standard deviation of

one degree, the maximum difference between the artificial value and I_{obs} was two degrees. However, an exception was allowed because the boundary between degrees V and VI (i.e. between non damage and damage) is particularly reliable: intensities less than V could not exceed VI, and intensities greater than VI could not be less than V. In setting these limits, an average of 37% of the I_{obs} was substituted for the two sets. In Table 3, two standard deviations were used as 95% probability errors. It should be noted that in 2004, we incorrectly referred to this randomization as a kind of bootstrap technique (Sirovich and Pettenati 2004; this misstatement was corrected in Pettenati and Sirovich 2007).

3.4 Isoseismal maps

Figures 5 and 7 show the results of the intensity surveys and our synthetic *pseudo-intensity* patterns generated with our bivariate natural-neighbour “N–N” interpolation pattern (Sirovich et al. 2002) based on Voronoi tessellation. We recall that the N–N isolines shown in the following figures are uniquely determined, that the N–N algorithm is deterministic, that it has non-adjustable parameters and that it has an all-pass filter character. In other words, it strictly adheres to the data, and the isolines are determined without any explicit or implicit assumption about the observed phenomenon. Therefore, everyone gets the same result. To plot the following N–N isoseismals, we used all data sites within a 0.1° -wide strip around the image shown (Figs. 5 and 7). Then, we inverted only the data within the shown areas.

Table 2 Range of the 11 source parameters in the inversion of the Ljubljana 1895 earthquake and the maximum allowable *pseudo-intensity*

Parameter	Explored range	Incremental variation step
Epicentre latitude ($^\circ$) N	45.80–46.20	0.01
Epicentre longitude ($^\circ$) E	14.15–14.75	0.01
Strike angle ($^\circ$)	0–359	1
Dip angle ($^\circ$)	30–90	1
Rake angle ($^\circ$)	0–179	1
Nucleation depth, H (km)	12–35	1
V_s (Km/sec)	3.50–3.95	0.01
Mach +	0.50–0.99	0.01
Mach -	0.50–0.99	0.01
Mo (dyne cm) 10^{25}	0.9–5	0.01
L +	0–20	1
L -	0–20	1
Maximum intensity allowed	10	

4 Earthquake inversion of the 14 April 1895 earthquake

Using *KF-NGA* inversion, we searched for 11 source-parameters of the study earthquake. Four hundred thirty one *MDPs* data were used, and the hyperspace of the residuals was examined with four demes of 1000 source models (the individuals in the genetic similarity); each source parameter (gene) was adjusted with the incremental variations given in Table 2. Of the 11 source parameters involved in the inversions, the epicentral coordinates and the angles that represent the fault plane solution are most sensitive: strike, dip and rake. Figure 5 shows

the isoseismals obtained by interpolating the used dataset with the N–N method. The data are included in the range: 45°.20N–46°.80N, 13°.30E–15°.70E. To best respect the data, we decided to treat the intermediate degrees (e.g. VI–VII) as half degrees (i.e. 6.5).

The “*D*” distance (see Section 3.2) is calculated by trial and error to prevent two demes from falling into the same minimum and to avoid that a deme is unable to reach the bottom of the depression of the hyperspace of residuals r_s if the *D* value is too large. Thus, we have assumed $D=0.088$. According to Ribarič (1982), the source depth can freely vary between 12 and 35 km. The hypocentral depth obtained from *KF-NGA* is considered an upper limit, since it is obtained in half-space condition.

After 1890 iterations, we obtained the solutions for four demes, as shown in Table 3.

The best solution of the source model is given by deme 2 with the minimum fitness, 281.0, and it has alpine orientation. Using the seismic moment value of $Mo=1.79 \cdot 10^{25}$ (dyne cm), the moment magnitude for this solution according to the empirical formula ($M=2/3 (\log Mo) - 10.7$) Hanks and Kanamori (1979) is $M=6.1$. Using the empirical relationship *M versus RLD* (Wells and Coppersmith 1994), we obtain a linear source of total length $L=15$ km, with 11 km along strike and

4 km antistrike. Figure 7 shows the N–N isoseismals of the *pseudo-intensities* of deme 2 in Table 3. The conjugate plane of deme 2 has strike = 107°, dip = 52°, rake = 93°, quite similar to those of the second solution (deme 1, Table 3).

The white box in Fig. 7 is the projection from the bilateral source at 29.7 km depth of deme 2 in Table 3; its nucleation is at the intersection of the two thin dotted lines. The virtual continuation of its plane, dipping 38° to NNE, intersects the topographic surface to the SSW (thick dashed segment), reported also on Fig. 2 (blue dashed line). Since the rake angle of deme 2 is next to $90^\circ \pm 180^\circ$ (Sirovich and Pette-nati 2004), we also show, in Fig. 7, the virtual out-cropping of the prosecution of the conjugate plane of deme 2 dipping 52° to SSE (see the thick dashed segment to the NNE). See also Section 5 in this regard. (Of course, faults with listric shapes often occur in nature and cannot be accounted for in our procedure).

In Fig. 7, the width of the source was calculated using the *M versus RW* relationship (Wells and Coppersmith 1994)

$$\log (RW) = 0.32M - 1.01 \quad (3)$$

And the dashed white lines are its projection onto the ground surface. It can be seen from Fig. 7 that the epicentre is located near the boundary between

Table 3 Results of inversion with the 4 demes

Parameters	Deme 1	Deme 2	Deme 3	Deme 4
Fitness	286.25	281.0	293.25	296.5
Epicentre latitude (°) N	46.04	46.04 ± 0.04	46.09	46.09
Epicentre longitude (°) E	14.38	14.41 ± 0.1	14.43	14.40
Strike angle (°)	98	282 ± 5	83	84
Dip angle (°)	52	38 ± 7	85	86
Rake angle (°) (± 180°)	87	86 ± 9	82	82
Nucleation depth, <i>H</i> (Km)	30.0	29.7 ± 5.0	29.9	30.0
<i>V_s</i> (Km/sec)	3.50	3.64 ± 0.16	3.76	3.60
Mach+	0.70	0.61 ± 0.07	0.61	0.70
Mach–	-0.56	-0.79 ± 0.05	-0.59	-0.71
<i>Mo</i> (dyne cm) 10 ²⁵	3.52	1.79 ± 1.08	4.94	3.15
<i>L</i> + ^a	12	11	7	19
<i>L</i> - ^a	8	4	16	1

Deme 2 gave the best fitness parameters. Deme 1, 3 and 4 have similar solutions, perhaps also due to the difficulties in calibrating the interdeme distance *D*

^aThe partial lengths are computed by *M versus RLD* (Wells and Coppersmith 1994); see Eq. 2

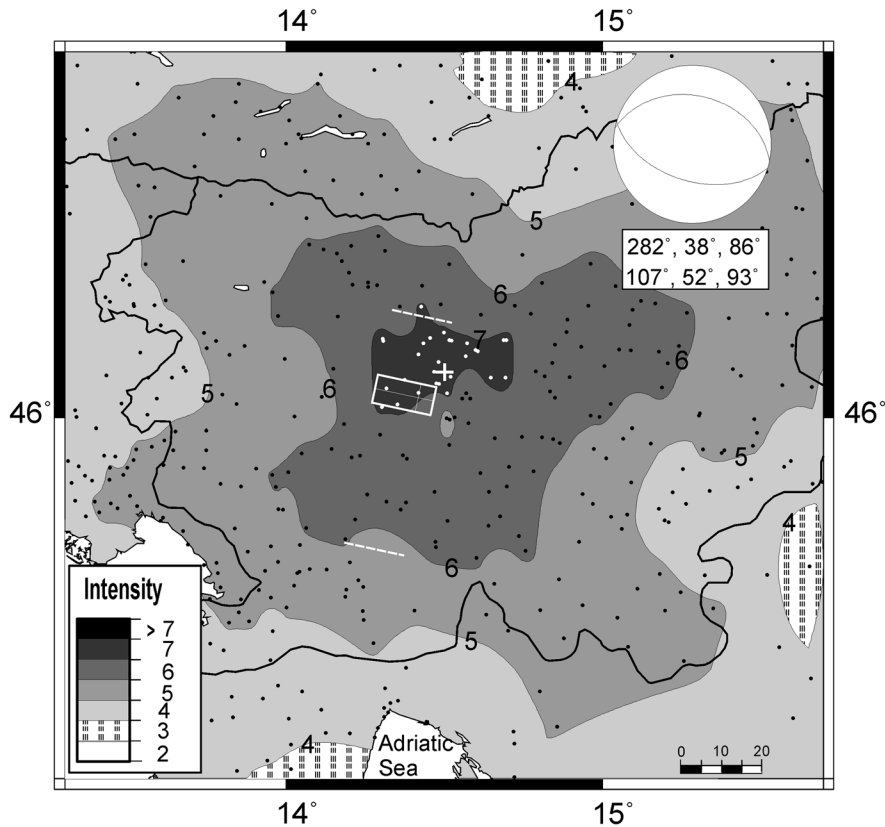


Fig. 7 Synthetic intensities (i.e. pseudo-intensities) generated by solving the absolute minimum variance solution deme 2 in column 3 of Table 3. You can see the parameters of deme 2 and its conjugate, under the beach ball. The white box is the projection of the bilateral source; its nucleation is at the intersection of the two thin dashed lines. The thick dashed segment to the south is the virtual intersection of the plane of deme

2 dipping 38° to the NNE, with the topographic surface; the same is true of the conjugate plane, which is dipping 52° to the SSW and thus appears virtually to the N. The beach ball is white because the *KF* method is not able to distinguish between the results of mechanisms that differ by 180° in the rake angle. The epicentre from Ribarič (1982) is marked with a white cross

pseudo-intensities 6 (grey) and 7 (dark grey). In particular, radiation patterns and directivity play a role in this.

The lobate shape of the synthetic isoseismals in Fig. 7 is typical of an almost pure dip-slip source (like deme 2 in Table 3). The N–N isoseismals of I_{obs} in Fig. 5 show preferential radiation-propagation in the E direction, namely from NE to SSE.

Recognition of similarities between the intensities in Figs. 5 and 7 is complicated by the inhomogeneous distribution of the observed data. In particular, the elongation of the area from VI degree toward E in Fig. 5 is influenced by some site effects of the alluvium in the Celje and Sava valleys (Fig. 2).

Note that the isoseismals of degree VII in Figs. 5 and 7 have approximately the same dimension.

5 Discussion

As mentioned above, the dataset of *MDPs* of the 1895 Ljubljana earthquake is a combination of two datasets: ARSO (2012) and CPTI15 (Rovida et al. 2020), using two different intensity scales (EMS-98 for the Slovenian and MCS for the Italian catalogue). Nevertheless, the two datasets match well in the area on the border between Italy and Slovenia (Fig. 5). The field is densely and uniformly sampled, so there are

no gaps. Therefore, *KF-NGA* was able to use a large number of data (431). The large dataset also allowed the use of 310 *MDPs* to examine local effects, all from the ARSO dataset and thus all in the EMS-98 scale. The 310 *MDP* values show site effects — such as the lower decay with the distance d for C1 alluvial sites compared to sites on rock or stiff soils — but likely also regional effects of uncertain origin. An interesting observation on Fig. 5 concerns the eastward extension of the area of V and VI with islands of VI–VII, which could affect the inversion — as in the Celje and Sava alluvium valleys (see also Fig. 2). For example, the *KF-NGA* inversion of the M 5.9 Whittier Narrows earthquake (Pettenati and Sirovich, 2003) dataset yielded a larger dip angle than the instrumentally determined one because the sites located above the Los Angeles Basin were amplified by the thick sedimentary cover.

Apart from the different intensity scales used (which is a minor issue here), we find differences between the sites studied in the mentioned countries. The ARSO dataset (2012) contains hundreds of *MDPs* for small villages and hamlets, as small rural inhabited villages were the typical urban settings in the region at the end of the nineteenth century. We have also reported findings from other studies such as those by Molnar et al. (2004) for the 2001 Nisqualli earthquake, where they observed a reduction in the resolving power of *MDPs* from street addresses (a full 1.0-unit difference in I) to zip codes (0.6-unit difference) and three-degree differences commonly found based on zip code. We have also examined some cases of differences between site and source effects. However, in the case of this earthquake, due to the limitations of our model, we cannot understand whether the above-mentioned three sites of VI in the meizoseismal area (see Section 2.3 and Fig. 5) may be due to the source (among other hypotheses, there is also the possibility that they may be due to different characteristics of the buildings compared to the surrounding villages).

Then, the intensities observed in small villages and hamlets likely represent the responses of small areas with a uniform geology. Instead, most of the I in the other catalogues belong to towns spread over large areas, and each *MDP* value represents the response of a large area with less uniform geologic condition. In this context, it is plausible that the seismic response of one soil is merged with the responses of other soils in the town.

The anomalous attenuation at sites between Slovenia and Croatia, at d greater than 50 km mentioned in Section 2.2, is worth discussing. See Fig. 3c; for example, the average sites d for the VI–VII degree increase relative to previous and subsequent I . In Fig. 5, it can be seen that the degrees V and VI iso-seismals extend more eastward than westward, with extensive islands of VI–VII at the eastern edge of the figure.

An earlier work by Suhadolc and Chiaruttini (1987) could perhaps provide an explanatory hypothesis for the high intensities observed in Fig. 5 to the E. These two authors studied the attenuation of PGAs between Slovenia and Croatia using synthetic seismograms and a series of laterally homogeneous lithospheric models. Note that the area studied by Suhadolc and Chiaruttini (1987) coincides with the one in Fig. 5, where the aforementioned anomalous behaviour of intensities towards the E is observed. The two authors note that the depth of the Moho, which decreases from 42 to 30 km from W to E (see also the map of Dezès et al. 2004), causes an anomalous peak of the PGA response between Slovenia and Croatia (i.e. east of the 15° E meridian in Fig. 5). In particular, Suhadolc and Chiaruttini (1987) found that for distances up to about 15° E in Fig. 5, the PGA peaks are due to the crustal Sg phase or to the sedimentary waves, depending on the depth of the source. East of 15° E in Fig. 5, the peak motion values are due to the S-wave reflection from the Moho, which is the initial part of the Lg wave group. In particular, the Slovenian sites with $I \geq VI$ located east of the E 15 meridian and the Croatian sites with $I \geq VI$ near the boundaries E and SE in Fig. 5 may be involved. Challenging hypotheses, however, is beyond the scope of the present work.

Despite the inhomogeneous distribution of the observed data, the solutions resulting from the *KF-NGA* inversion are consistent with the more obvious tectonic features in the Ljubljana area. In fact, the strike of 282°, accompanied by the rake of 86 ± 180 (deme 2 in Table 3), is consistent with the WNW-oriented Dinaric structures. Considering that the area is affected by the internal Dinaric Balkan thrusts and the two external thrusts (paragraph 1.2), the dip of the solution is a bit too high to justify the origin of the thrust. The tectonic interpretation is not straightforward, as the studies under Ljubljana indicate a low-angle thrust. As in the previous article on the 1987 Whittier Narrows

earthquake (Pettenati and Sirovich, 2003), we can hypothesise that the high value of the obtained dip angle could be influenced by local effects of the valleys east of the epicentre, as mentioned above. However, the relatively high errors of rake and dip angles of the deme 2 in Table 3 emphasise the uncertainties described. Instead, the relative stability of strike angle and epicentral coordinates is noteworthy. The depth is also subject to high errors, but it should be kept in mind that the reliability of this parameter is also low because *KF* uses an elastic half-space. Assuming a thrust mechanism and considering the depth of 16 km given by Ribarič (1982) in Table 1, the causative fault could be the Hrušica nappe or the Snežnik thrust fault (Fig. 2), southwest of Ljubljana (Placer et al. 2010). In previous inversions of the *KF-NGA* method, we have obtained results consistent with the tectonic context, even in situations where sampling is constrained by the presence of the sea (see Loreto et al. 2012).

Tiberi et al. (2018) also attempted to obtain a result for the 1895 Ljubljana earthquake, but with a different approach. They consider nine source models (Fig. 2), derived from real known faults and from the ones previously identified by *KF-NGA* and reported in some presentations by Jukić et al. (2011, 2012) and also in the Master thesis by Jukić (2011; erroneously dated 2009 in Tiberi et al. 2018). Among the source models considered by Tiberi et al. (2018), the Vodice N fault, north of Ljubljana (Jamšek Rupnik et al. 2013; Jukić 2011), is close to the Dinaric trend, while Vodice S and the two segments of the Vič fault (Verbič, 2006) are WSW-ENE oriented (see Fig. 2). Tiberi et al. (2018) also consider five strike-slip faults with NNW-SSE direction (Borovnica, Mišjedolski, Želumlje, Ortnek and Dobropolje; Moulin et al. 2016) located further south of the Ljubljana urbanized area (Fig. 2).

Following their approach, Tiberi et al. (2018) calculate peak ground velocities using different ground motion prediction equations (GMPEs) and synthetic seismograms, obtaining a set of ground motion scenarios. Then, they compare the obtained scenarios qualitatively and quantitatively with the reference macroseismic intensity database (the quantitative comparison is made using ad hoc ground motion to intensity conversion equations, GMICEs). They distinguish between the different sources and configurations assumed for each scenario and find a slight prevalence, as best source model, of the Ortnek fault about 10 km SSE of Ljubljana.

In Section 3.1, we described the ambiguity of the rake angle in the *KF-NGA* method, regarding the impossibility to distinguish the mechanism that differs in the rake angle by 180 and in the case of pure dip-slip mechanisms. We have seen that the solutions of deme 1 and 2 in Table 3 coincide with the conjugate planes of the same mechanism. Therefore, deme 1 can also be a direct fault (rake $87 + 180 = 267^\circ$), whose virtual intersection with the surface almost coincides with the Vodice faults (see the blue dashed segment in Fig. 2, near Kranj). At this point, the situation becomes intriguing. Because Vrabc (2001) had assigned the north fault a normal mechanism with southward dip, and also Jamšek Rupnik (2013), who interpreted the Vodice faults as reverse, admits that the presence of active reverse faults in the centre of the Ljubljana Basin is one of the most interesting geological and geomorphological puzzles of the Ljubljana Basin. Thus, we think that the assumption of a normal movement with an ENE-WSW solution for deme 1 (Table 3) is not precluded. The blue dashed intersection in Fig. 2 is located about 2 km N of the slope of Vodice N; however, as mentioned above, real faults have a listric shape, so, the aforementioned intersection of deme 1 could well be located even a few kilometres south of the Vodice faults.

6 Conclusions

The dataset for the earthquake that occurred in the urban area of Ljubljana (Slovenia) on 14 April 1895 shows a rather inhomogeneous intensity distribution. Site effects are statistically detected in the 310 qualified Slovenian macroseismic data points (Pettenati et al. 2012), showing effects due to the type of soils, such as lower decay with the distance for C1 alluvial sites than on rock or stiff soils. This has already been noted for other datasets by Pettenati and Sirovich (2007). In addition, some site effects on the border with Croatia have not yet been clarified. Nevertheless, the *KF-NGA* method provided interesting solutions. The two proposed solutions, consistent with conjugate planes of the same focal mechanism, are compatible with the seismotectonic framework of the area. The first solution (strike 282° , dip 38° , rake 86°) would belong to the Dinaric thrusts system, oriented WNW-ESE. Its virtual upward extension would roughly correspond to the External Dinaric Thrust Belt found southwest of Ljubljana. In particular, this

solution would be compatible with the Hrušica and Snežnik thrust (Placer et al. 2010). The virtual outcrop of the second one (Deme 1 in Table 3: 98°, 52°, 87°), dipping southward (see Figs. 7 and 2), almost coincides with the mapped outcrop of the only structure considered active in the Ljubljana basin to the northwest of the capital: the Vodice faults, for which an interpretation as normal fault is not excluded.

Spreadsheet1: Excel file with the list of 1004 MDPs with state abbreviation, intensity value, latitude, longitude, State, site name.

Acknowledgements We are grateful to Romano Camassi and Andrea Tertulliani for the helpful discussions about MCS and EMS-98 intensity scales. Thanks are due to Riccardo Percacci for the English review and an aid with the dataset organization. We would also like to thank the two reviewers for their excellent work.

Author contribution Franco Pettenati designed and developed the *KF* method and the software, contributed to the statistical analysis and wrote the first draft of the article. He revised all the text after the referee observations.

Ivana Jukić performed the inversion and contributed to the statistical analysis.

Livio Sirovich designed and developed the *KF* method, performed the statistical analysis and the interpretation; he provided an overall revision of the manuscript.

Ina Cević is the author of the used macroseismic dataset and reviewed the manuscript.

Giovanni Costa reviewed and approved the manuscript.

Peter Suhadolc proposed the study and proofread the manuscript.

Funding Open access funding provided by Istituto Nazionale di Oceanografia e di Geofisica Sperimentale within the CRUI-CARE Agreement.

Data availability The macroseismic Italian data are available in the INGV CPTI15 (Rovida et al. 2020) catalogue, the macroseismic data of Slovenia and other countries are available in AHEAD (Albini et al. 2013), and the soil classification data are available upon request to the authors.

Declarations

Competing interests The authors declare no competing interests.

Disclaimer The views expressed by the authors do not necessarily reflect those of the CTBTO Preparatory Commission.

Open Access This article is licensed under a Creative Commons Attribution 4.0 International License, which permits use, sharing, adaptation, distribution and reproduction in any medium or format, as long as you give appropriate credit to the

original author(s) and the source, provide a link to the Creative Commons licence, and indicate if changes were made. The images or other third party material in this article are included in the article's Creative Commons licence, unless indicated otherwise in a credit line to the material. If material is not included in the article's Creative Commons licence and your intended use is not permitted by statutory regulation or exceeds the permitted use, you will need to obtain permission directly from the copyright holder. To view a copy of this licence, visit <http://creativecommons.org/licenses/by/4.0/>.

References

- Albini P, Locati M, Rovida A, Stucchi M (2013) European Archive of Historical Earthquake Data (AHEAD). Istituto Nazionale di Geofisica e Vulcanologia (INGV). <https://doi.org/10.6092/ingv.it-ahead>
- ARSO (2012) Data availability ARSO 2012 macroseismic archive. Agencija Republike Slovenije za Okolje, Ljubljana, Slovenia. Electronic database
- Atanackov J, Jamšek Rupnik P, Jež J, Celarc B, Novak M, Milanič B, Markelj A, Bavec M, Kastelic V (2021) Database of active faults in Slovenia: compiling a new active fault database at the junction between the Alps, the Dinarides and the Pannonian Basin tectonic domains. *Front Earth Sci* 9(604388):1–21. <https://doi.org/10.3389/feart.2021.604388>
- Bajc J, Aoudia A, Sarač A, Suhadolc P (2001) The 1998 Bovec - Krn mountain (Slovenia) earthquake sequence. *Geophys Res Lett* 28:1839–1842. <https://doi.org/10.1029/2000GL011973>
- Barnett V, Lewis T (1978) Outliers in statistical data. Wiley series in Probability and Mathematical Statistics. Applied Probability and Statistics. Wiley, Chichester
- Bavec M, Ambrožič T, Atanackov J, Cević I, Celarc B, Gosar A, Jamšek P, Jež J, Kogoj D, Koler B, Kuhar M, Milanič B, Novak M, Pavlovčič Prešeren P, S. Savšek S, Sterle O, Stopar B, Vrabc M, Zajc M, and Živčič M (2012) Some seismotectonic characteristics of the Ljubljana Basin, Slovenia. *Geophysical Research Abstracts* Vol. 14, Poster A498, EGU2012-9370. EGU General Assembly 2012
- Camassi R, Caracciolo CH, Castelli V, Slejko D (2011) The 1511 eastern Alps earthquakes: a critical update and comparison of existing macroseismic datasets. *J Seismol* 15:191–213
- Cević I (1998) Investigation of earthquakes (1400–1899) in Slovenia. Internal report for the BEECD project, Seismological Survey, Ljubljana
- Cević I (1998) Potres v Ljubljani 15. julija 1897. In: J. Lapajne (ed.), *Potresi v Sloveniji leta 1997*, URSG, Ljubljana, 43–57. http://potresi.arso.gov.si/doc/dokumenti/porocila_in_publikacije/potresi_v_letu_1997.pdf
- Cornell CA (1968) Engineering seismic risk analysis. *Bull Seismol Soc Am* 58:1583–1606
- Del Mese S, Graziani L, Meroni F, Pessina V, Tertulliani A (2023) Considerations on using MCS and EMS-98 macroseismic scales for the intensity assessment of contemporary Italian earthquakes. *Bull Earthq Engng* 21:4167–4189. <https://doi.org/10.1007/s10518-023-01703-0>

- Dezès P, Schmid SM, Ziegler PA (2004) Evolution of the European Cenozoic Rift System: interaction of the Alpine and Pyrenean orogenes with their foreland lithosphere. *Tectonophysics* 389:1–33
- Fitzko F, Suhadolc P, Aoudia A, Panza GF (2005) Constraints on the location and mechanism of the 1511 western-Slovenia earthquake from active tectonics and modelling of macroseismic data. *Tectonophysics* 404:77–90
- Frankel A (1995) Mapping seismic hazard in the central and eastern United States. *Seism Res Lett* 66(4):8–21
- Gasparini P, Vannucci G, Tripone D, Boschi E (2010) The location and sizing of historical earthquakes using the attenuation of macroseismic intensity with distance. *Bull Seismol Soc Am* 100:2035–2066. <https://doi.org/10.1785/0120090330>
- Gentile F, Pettenati F, Sirovich L (2004) Validation of the automatic nonlinear source inversion of the U.S. Geological Survey intensities of the Whittier Narrows, 1987 earthquake. *Bull Seism Soc Am* 94(5):1737–1747
- Grünthal G, Wahlström R (2012) The European-Mediterranean Earthquake Catalogue (EMEC) for the last millennium. *J Seismol* 16:53–570
- Grünthal G, ed. (1998) European Macroseismic Scale 1998 https://gfzpublic.gfz-potsdam.de/rest/items/item_227033_4/component/file_227032/content
- Grützner C, Aschenbrenner S, Jamšek Rupnik P, Reicherter K, Saifelislam N, Vičić B, Vrabec M, Welte J, Ustaszewski K (2021) Holocene surface rupturing earthquakes on the Dinaric Fault System, western Slovenia, *Solid Earth Discussion: Open Access Preprint*. <https://doi.org/10.5194/se-2021-7>
- Hanks TC, Kanamori H (1979) A moment magnitude scale. *J Geophys Res* 84:2348–2350
- Herak D, Herak M, Tomljenović B (2009) Seismicity and focal mechanisms in North-Western Croatia. *Tectonophysics* 465:212–220. <https://doi.org/10.1016/j.tect.2008.12.005>
- Jamšek Rupnik P, Benedetti L, Preusser F, Bavec M, Vrabec M (2013) Geomorphic evidence of recent activity along the Vodice thrust fault in the Ljubljana Basin (Slovenia) – a preliminary study. *Ann Geophys* 56:680–688
- Jamšek Rupnik P, Atanackov J, Skaberne D, Jež J, Milanič B, Novak M, Lowick S, Bavec M (2015) Paleoseismic evidence of the Vodice fault capability (Ljubljana Basin, Slovenia). 6th International INQUA Meeting on Paleoseismology, Active Tectonics and Archaeoseismology, 19–24 April 2015, Pescina, Fucino Basin, Italy, p 4, paleoseismicity.org
- Jamšek Rupnik, P (2013) Geomorphological evidence of active tectonics in the Ljubljana Basin. 125 Doctoral Dissertation. Ljubljana, UL FGG, UL NTF, Doctoral study Built Environment, Scientific area Geology, University of Ljubljana
- Jukić I (2011) The focal mechanisms of the 1895 Ljubljana earthquake and of its 1897 strong aftershock from the inversion of their macroseismic fields. University of Trieste, Master Thesis
- Jukić I, Pettenati F, Sirovich L, Suhadolc P (2011) Parametri di sorgente dei terremoti di Ljubljana (Slovenia) del 1895 e del 1897 dalla i inversione di dati macrosismici. Gruppo Nazionale di Geofisica della Terra solida (GNGTS), 30° Convegno Nazionale, 14–17.11.2011 Trieste (Italy), Abstracts: 57-59
- Jukić I, Suhadolc P, Pettenati F, Sirovich L, Jamšek Rupnik P, Cević I (2012) Macroseismic data of the Ljubljana (Slovenia) 1895 earthquake and its 1897 aftershock and their inversion for source parameters. 33-rd General Assembly of the European Seismological Commission (GA ESC 2012), August 19–24, 2012, Moscow, Russia
- Kay M (1937) Stratigraphy of the Trenton Group. *Geol Soc Am Bull* 48:233–302
- Koper KD, Wyssession ME, Wiens DA (1999) Multimodal function optimization with a niching genetic algorithm. *Bull Seism Soc Am* 89:978–988
- Lapajne J, Šket-Motnikar B, Zupančič P (2003) Probabilistic seismic hazard assessment methodology for distributed seismicity. *Bull Seism Soc Am* 93(6):2502–2515
- Levine D (1996). Users guide to the PGAPack parallel genetic algorithm library, Rep. Argonne National Laboratory ANL-95/18:73, Argonne, IL
- Loreto MF, Zgur F, Facchin L, Fracassi U, Pettenati F, Tomini I, Burca G, Cossarini M, De Vittor C, Sandron D, the Explora technicians team (2012) In search of new imaging for old earthquakes: new geophysical survey offshore Calabria (southern Tyrrhenian sea, Italy). *Boll Geof Teor Appl* 53(4):385–401. <https://doi.org/10.4430/bgta0046>
- Madariaga R, Bernard P (1985) Ray theoretical strong motion synthesis. *J Geophys* 58:73–81
- Martin LS, Scales JA, Fischer TL (1992) Global search and genetic algorithms. *The Lead Edge* 2:22–26
- Molnar S, Cassidy JF, Dosso SE (2004) Comparing intensity variation of the 2001 Nisqually Earthquake with geology in Victoria, British Columbia. *Bull Seism Soc Am* 94:2229–2238
- Moulin A, Benedetti L, Rizza M, Jamšek Rupnik P, Gosar A, Bourlès D, Keddadouche K, Aumaître G, Arnold M, Guillou V, Ritz J-F (2016) The Dinaric fault system: large-scale structure, rates of slip and Plio-Pleistocene evolution of the transpressive northeastern boundary of the Adria microplate. *Tectonics* 35(10):2258–2292. <https://doi.org/10.1002/2016TC004188>
- Musson R, Grünthal G, Stucchi M (2010) The comparison of macroseismic intensity scales. *J Seismol* 14:413–428. <https://doi.org/10.1007/s10950-009-9172-0>
- Paolucci R, Aimar M, Ciancimino A, Dotti M, Foti S, Lanzano G, Mattevi P, Pacor F (2021) Vanin M (2021) Checking the site categorization criteria and amplification factors of the 2021 draft of Eurocode 8 Part 1–1. *Bull Earthq Engng* 19:4199–4234
- Pettenati F, Sirovich L (2003) Test of source-parameter inversion of the U.S. Geological Survey intensities of the Whittier Narrows, 1987 earthquake. *Bull Seism Soc Am* 93(1):47–60
- Pettenati F, Sirovich L (2007) Validation of the intensity-based source inversions of three destructive California earthquakes. *Bull Seism Soc Am* 97(5):1587–1606. <https://doi.org/10.1785/0120060169>
- Pettenati F, Sirovich L, Sandron D (2018) The usage of the regional pattern of damage (intensity) to retrieve informations of 6 May 1976 M6.4 earthquake. *Boll Geofis Teor Appl* 59:445–462. <https://doi.org/10.4430/bgta0250>

- Pettenati F, Sirovich L, Jamsek P (2012) Modern uses of intensities: site effects in Slovenia in 1895; source inversion of an intermediate earthquake of 1909 in the Po Valley; damage scenario of a small earthquake of 2011 in NW Italy. Proc. 33rd General Assembly of the European Seismological Commission ESC 2012, Aug. 19–24, Moscow, Symp. NIS-1: 335
- Placer L (2008) Principles of the tectonic subdivision of Slovenia. *Geologija* 51(2):205–217. <https://doi.org/10.5474/geologija.2008.021.ISSN0016-7789>
- Placer L, Vrabec M, Celarc B (2010) The bases for understanding of the NW Dinarides and Istria Peninsula tectonics. *Geologija* 53(1):55–86. <https://doi.org/10.5474/geologija.2010.005>
- Poljak M, Živčič M, Zupančič P (2000) The seismotectonic characteristics of Slovenia. *Pure Appl Geophys* 157:37–55
- Ribarič V (1982) Seismicity of Slovenia, catalog of earthquakes (792 A.D. - 1981). Seizmološki zavod Socialistične Republike Slovenije, Publ. Series A, n. 1–1, Ljubljana, Slovenia, 650
- Rovida A, Locati M, Camassi R, Lolli B, Gasperini P (2020) The Italian earthquake catalog CPTI15. *Bull Earthq Engng* 18(7):2953–2984. <https://doi.org/10.1007/s10518-020-00818-y>
- Sirovich L (1996) A simple algorithm for tracing synthetic isoseismals. *Bull Seism Soc Am* 86:1019–1027
- Sirovich L (1997) Synthetic isoseismals of three earthquakes in California Nevada. *Soil Dyn and Earthq Engng* 16:353–362
- Sirovich L, Pettenati F (2004) Source inversion of intensity patterns of earthquakes; a destructive shock of 1936 in northeast Italy. *J Geoph Res* 109(B10309):16. <https://doi.org/10.1029/2003JB002919>
- Sirovich L, Pettenati F, Chiaruttini C (2001) Test of source-parameter inversion of intensity data. *Nat Hazards* 24:105–131
- Sirovich L, Pettenati F, Cavallini F, Bobbio M (2002) Natural-neighbor isoseismals. *Bull Seism Soc Am* 92:1933–1940
- Sirovich L, Pettenati F, Sandron D (2009) Source- and site-effects in the intensities of the M5.4 July 29, 2008 earthquake in South Los Angeles. *Seism Res Lett* 80(6):936–945. <https://doi.org/10.1785/gssrl.80.6.967>
- Sirovich L, Pettenati F, Cavallini F (2013) Intensity-based source inversion of a destructive earthquake of 1694 in the southern Apennines, Italy. *J Geoph Res* 118:1–17. <https://doi.org/10.1002/2013JB010245>
- Sirovich L, Pettenati F, Buseti M (2012). The problem of earthquake-capable faults and maximum related magnitudes for two critical facilities in Italy and in Slovenia. Proc. 33rd General Assembly of the European Seismological Commission ESC 2012, Aug. 19–24, Moscow, Symp. NIS-3, 350
- Šket-Motnikar B, Zupančič P, Živčič M, Atanackov J, Jamšek Rupnik P, Čarman M, Danciu L, Gosar A (2022) The 2021 seismic hazard model for Slovenia (SHMS21): overview and results. *Bull Earthq Engng* 20:4865–4894
- Suhadolc P, Chiaruttini C (1987) A theoretical study of the dependence of the peak ground acceleration of source and structure parameters. In: Erdik MO, Toksoz MO (eds) *Strong Ground Motion Seismology*. Reidel, Dordrecht, pp 143–183
- Tiberi L, Costa G, Jamšek Rupnik P, Cević I, Suhadolc P (2018) The 1895 Ljubljana earthquake: can the intensity data points discriminate which one of the nearby faults was the causative one? *J Seismol* (2018) 22:927–941. <https://doi.org/10.1007/s10950-018-9743-z>
- Vannucci G, Lolli B, Gasperini P (2021) Inhomogeneity of macroseismic intensities in Italy and consequences for macroseismic magnitude estimation. *Seismol Res Lett* 92:2234–2244. <https://doi.org/10.1785/0220200273>
- Verbič T (2006) Aktivni reverzni prelomi med Ljubljano in Kranjem = Quaternary-active reverse faults between Ljubljana and Kranj, central Slovenia. *Razprave IV Razreda SAZU* 47(2):101–142
- Vičič B, Aoudia A, Javed F, Foroutan M, Costa G (2019) Geometry and mechanics of the active fault system in western Slovenia. *Geoph J Int* 217:1755–1766
- Vrabec M, Fodor L (2006) Late Cenozoic tectonics of Slovenia: structural styles at the Northeastern corner of the Adriatic microplate. In: *The Adria microplate: GPS geodesy, tectonics and hazards*, Pinter N., Grenczy G., Weber J., Stein S. and Medak D. (eds), NATO Sci Ser IV, Earth Environ Sci, 61:151–168
- Vrabec M (2001) Strukturna analiza cone Savskega preloma med Trstenikom in Stahovico. PhD thesis. Ljubljana, University of Ljubljana, Faculty of Natural Sciences and Engineering, Department of Geology: 94 p.
- Wells DL, Coppersmith KJ (1994) New empirical relationships among magnitude, rupture length, rupture width, rupture area, and surface displacement. *Bull Seism Soc Am* 84:974–1002
- Žibret L, Vrabec M (2016) Palaeostress and kinematic evolution of the orogen-parallel NW-SE striking faults in the NW External Dinarides of Slovenia unraveled by mesoscale fault-slip data analysis, *Geologia Croatica*. *J Croat Geol Surv Croat Geol Soc* 69(3):295–305

Publisher's Note Springer Nature remains neutral with regard to jurisdictional claims in published maps and institutional affiliations.